J. Fluid Mech. (2009), *vol.* 629, *pp.* 173–193. © 2009 Cambridge University Press
doi:10.1017/S002211200900651X Printed in the United Kingdom

Drag and lift forces acting on a spherical gas bubble in homogeneous shear liquid flow

KEN-ICHI SUGIOKA[1] AND SATORU KOMORI[2]†

[1]Department of Chemical Engineering, Osaka Prefecture University, Sakai 599-8531, Japan

[2]Department of Mechanical Engineering and Science and Advanced Institute of Fluid Science and Engineering, Kyoto University, Kyoto 606-8501, Japan

(Received 4 June 2008 and in revised form 4 February 2009)

Drag and lift forces acting on a spherical gas bubble in a homogeneous linear shear flow were numerically investigated by means of a three-dimensional direct numerical simulation (DNS) based on a marker and cell (MAC) method. The effects of fluid shear rate and particle Reynolds number on drag and lift forces acting on a spherical gas bubble were compared with those on a spherical inviscid bubble. The results show that the drag force acting on a spherical air bubble in a linear shear flow increases with fluid shear rate of ambient flow. The behaviour of the lift force on a spherical air bubble is quite similar to that on a spherical inviscid bubble, but the effects of fluid shear rate on the lift force acting on an air bubble in the linear shear flow become bigger than that acting on an inviscid bubble in the particle Reynolds number region of $1 \leqslant Re_p \leqslant 300$. The lift coefficient on a spherical gas bubble approaches the lift coefficient on a spherical water droplet in the linear shear air-flow with increase in the internal gas viscosity.

1. Introduction

The dispersion phenomena of gas bubbles are seen not only in industrial plants such as the bubble columns but also in environmental flows such as the whitecaps generated by intensive wave breaking. It is of great importance to precisely estimate heat and mass transfer across the air–water interface of an air bubble such as entrained bubbles under the air–sea interface with intensive wave breaking in developing a reliable climate model. In order to estimate such heat and mass transfer, we have to understand the motions outside and inside a gas bubble and the effects of mean shear on fluid forces acting on a gas bubble.

When a rigid sphere or a fluid sphere is moving in a shear flow, transverse force is exerted as lift force. The shear of the ambient flow is considered one of the factors affecting on the lift force on a spherical bubble. The shear-induced lift force on a rigid sphere acts towards the higher-fluid-velocity side from the lower-velocity side (Saffman 1965; Dandy & Dwyer 1990; McLaughlin 1993). Komori & Kurose (1996) and Kurose & Komori (1999) first performed three-dimensional direct numerical simulation (DNS) for the flow field outside a rigid sphere in the range of the particle Reynolds number of $Re_p = 1 - 500$. Here, Re_p is defined by $U_c d/\nu$, where d is the diameter of a sphere, U_c the fluid velocity on the streamline through the centre of a sphere and ν the kinematic viscosity. They found that the direction of the lift

† Email address for correspondence: komori@mech.kyoto-u.ac.jp

force acting on a stationary rigid sphere at higher Re_p is opposite that predicted by the inviscid and low-Reynolds-number theories, owing to the flow separations behind a sphere. The same behaviour of the lift force on a stationary rigid sphere was also reported by the DNS of Bagchi & Balachandar (2002). On the other hand, the shear-induced lift force on a bubble for high particle Reynolds numbers has been discussed by numerical simulations. Legendre & Magnaudet (1998) and Kurose, Misumi & Komori (2001) computed the lift force acting on an inviscid bubble in a viscous flow by using DNSs. They found that the flow separation behind an inviscid sphere does not appear and that the lift force on an inviscid bubble acts towards the higher-fluid-velocity side from the lower-velocity side.

In the above-mentioned studies, only the flow field outside a rigid sphere or an inviscid sphere has been considered in a uniform shear flow. However, in the case of a fluid sphere like a spherical droplet and a bubble, it is necessary to consider the flow fields both outside and inside a fluid sphere. For a linear shear creeping flow ($Re_p \ll 1$), the flow fields outside and inside a spherical bubble have been analysed by the Legendre & Magnaudet (1997) by using Saffman's low-Reynolds-number theory (Saffman 1965). For moderate and high particle Reynolds numbers ($Re_p > 1$), Sugioka & Komori (2007) conducted the three-dimensional DNS of flows inside and outside a spherical water droplet and estimated drag and lift forces. They found that the behaviour of the lift force on a water droplet is similar to that on a rigid sphere and that the viscous lift on a spherical droplet is smaller than that on a rigid sphere at the same Re_p, whereas the pressure lift becomes larger. However, three-dimensional DNS of flows both inside and outside a spherical gas bubble has not been conducted, and the effect of the flow inside a gas bubble on the lift force has not been clarified. On the other hand, the numerical simulation of flow inside and outside both a two-dimensional cylindrical bubble and a three-dimensional spherical bubble was conducted using the lattice Boltzmann method (Sankaranarayanan, Shan & Kerekidis 2002; Sankaranarayanan & Sundaresan 2002). However, the lift force on a three-dimensional spherical bubble has not been estimated.

The purpose of this study is to investigate the effects of the fluid shear on drag and lift forces acting on a spherical gas bubble in a viscous linear shear liquid flow with moderate and high particle Reynolds numbers by applying a three-dimensional DNS to flows both inside and outside a gas bubble and to clarify the effect of viscous flow inside a gas bubble on lift force.

2. Direct numerical simulation

The flow geometry and coordinate system for computations are shown in figure 1. The flow geometry and coordinate system for computations are the same as in the authors' previous paper (Sugioka & Komori 2007). In this study, cylindrical coordinates (x, r, θ) were used. The ambient flow around a bubble was a linear shear flow, given in a dimensionless form by

$$U = 1 + \alpha y. \tag{2.1}$$

Here, α is the dimensionless fluid shear rate of the mean flow defined by

$$\alpha = \frac{\partial U}{\partial y}\frac{d}{U_c}, \tag{2.2}$$

where $\partial U/\partial y$ is the dimensional fluid shear rate of the mean flow.

	Case 1	Case 2	Case 3	Case 4
μ_o/μ_i	48.95	489.5	9.790	4.895
ρ_o/ρ_i	841.4	841.4	841.4	841.4

TABLE 1. Fluid properties.

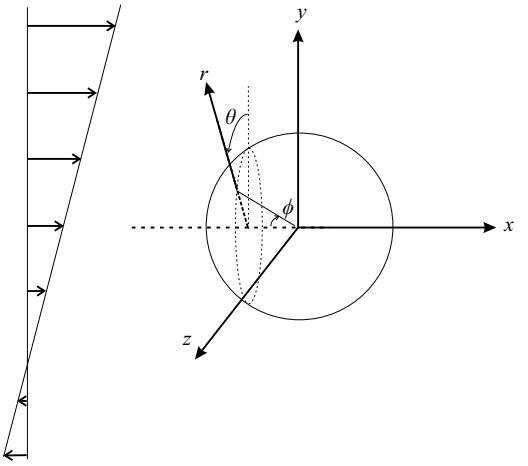

FIGURE 1. Coordinate system for a spherical bubble.

Table 1 shows the physical properties of fluids outside and inside a gas bubble. Here, μ is the viscosity and ρ is the density of the fluid. The subscripts o and i indicate the ambient fluid outside a bubble and the fluid inside a bubble, respectively. In case 1, the viscosity and density ratios correspond to an air bubble in water. In addition, the values of the viscosity ratio in cases 2, 3 and 4 are set to 10, 0.2 and 0.1 times that of an air bubble in water, respectively. These values correspond to gas bubbles with 0.1, 5 and 10 times the air viscosity in water flow or air bubbles in the liquid flow with 10, 0.2 and 0.1 times the water viscosity, respectively.

In the case of an air bubble in the water flow, the capillary number ($\mu U_c/\sigma$) and the Weber number ($\rho U_c^2 d/\sigma$) respectively were 2.5×10^{-3} and 0.50 at most for $Re_p \leqslant 100$. Here, σ denotes the surface tension. At $Re_p = 300$, the capillary number and the Weber number were 5.0×10^{-3} and 3.01, respectively. From these values of the capillary and the Weber number for $Re_p \leqslant 100$, it is understood that the deformation of the bubble from a spherical shape and the force owing to the deformation are negligibly small (Wohl & Rubinow 1974; Leal 1980). Therefore, to clarify the contributions of the fluid shear and the flow inside a bubble on the fluid force, it is here assumed that a bubble keeps a spherical shape. In addition, it is well known that the surface mobility of a bubble in water flow is influenced by impurities which create a gradient in surface tension. The effect changes the boundary condition effectively to a no-slip condition at the bubble interface (Fdhila & Duineveld 1996; Maxworthy *et al.* 1996; Palaparthi, Demetrios & Maldarelli 2006). However, bubbles in methanol and silicone oil are not influenced by the impurities (Takemura & Yabe 1998, 1999). The purpose of this study is to clarify the fluid force on spherical gas bubbles in liquid flows with different viscosity ratios and the effect of the internal gas flow on the fluid force. To focus this subject, the influence of the impurity in water will not be discussed here.

The governing equations are the continuity equation and the Navier–Stokes (NS) equations. The continuity equation is given by

$$\nabla \cdot \boldsymbol{V} = 0. \tag{2.3}$$

Here, $\boldsymbol{V}(=(U, V, W))$ denotes the velocity vector. The three-dimensional NS equations in cylindrical coordinates are given by

$$\frac{\partial U}{\partial t} + (\boldsymbol{V} \cdot \nabla)U = -\frac{\partial p}{\partial x} + \frac{1}{Re_{p,k}}\nabla^2 U, \tag{2.4}$$

$$\frac{\partial V}{\partial t} + (\boldsymbol{V} \cdot \nabla)V - \frac{W^2}{r} = -\frac{\partial p}{\partial r} + \frac{1}{Re_{p,k}}\left(\nabla^2 V - \frac{V}{r^2} - \frac{2}{r^2}\frac{\partial W}{\partial \theta}\right), \tag{2.5}$$

$$\frac{\partial W}{\partial t} + (\boldsymbol{V} \cdot \nabla)W + \frac{VW}{r} = -\frac{1}{r}\frac{\partial p}{\partial \theta} + \frac{1}{Re_{p,k}}\left(\nabla^2 W - \frac{W}{r^2} + \frac{2}{r^2}\frac{\partial V}{\partial \theta}\right). \tag{2.6}$$

In our previous paper (Sugioka & Komori 2007), the third term on the left hand side of the radial component of the NS equation has a typographical error. The particle Reynolds number $Re_p(=\rho U_c d/\mu)$ is based on the mean velocity of the ambient fluid on the stream through the centre of the bubble, U_c. Here, d is the diameter of a bubble. The particle Reynolds number outside a bubble $Re_{p,o}$ and the particle Reynolds number inside a bubble $Re_{p,i}$ are not independent and are related by

$$Re_{p,i} = \frac{\rho_i}{\rho_o}\frac{\mu_o}{\mu_i}Re_{p,o}. \tag{2.7}$$

The NS equations were directly solved using a finite-difference scheme based on the marker and cell (MAC) method. The numerical procedure used here was first developed by Hanazaki (1988) and is essentially the same as used in Komori & Kurose (1996), Kurose & Komori (1999), Kurose *et al.* (2001) and Sugioka & Komori (2007).

The boundary conditions for a spherical bubble are same as that for a spherical droplet in the authors' previous paper (Sugioka & Komori 2007). In this study, it is assumed that the effect of surfactant on the bubble surface is neglected. In order to compare the fluid forces acting on a spherical gas bubble with those on a spherical inviscid bubble, the velocity field around an inviscid bubble was computed by using the same DNS. In this case, the boundary conditions on the surface of an inviscid bubble were given by a slip condition.

The fluid force acting on a spherical bubble is estimated by integrating the pressure and viscous stresses over the surface of a spherical bubble. The components in the streamwise direction (x-direction) and the direction normal (y-direction) to the streamwise direction of the fluid forces are the drag and lift forces. The drag and lift coefficients C_D and C_L are defined using the projected area of a spherical bubble as follows:

$$C_D + C_L = \frac{\boldsymbol{e_x} \cdot \left(\int_S -p\boldsymbol{e_n}\,\mathrm{d}S + \int_S \boldsymbol{\tau}\,\mathrm{d}S\right)}{\frac{1}{2}\pi\rho_o U_c^2\left(\frac{d}{2}\right)^2} + \frac{\boldsymbol{e_y} \cdot \left(\int_S -p\boldsymbol{e_n}\,\mathrm{d}S + \int_S \boldsymbol{\tau}\,\mathrm{d}S\right)}{\frac{1}{2}\pi\rho_o U_c^2\left(\frac{d}{2}\right)^2}. \tag{2.8}$$

Here, $\boldsymbol{e_x}$ and $\boldsymbol{e_y}$ are the unit vectors in x- and y-direction and $\boldsymbol{e_n}$ is the unit vector normal to the surface of a bubble. The definition of the lift coefficient used in this study is the same as that by Dandy & Dwyer (1990) and Bagchi & Balanchandar

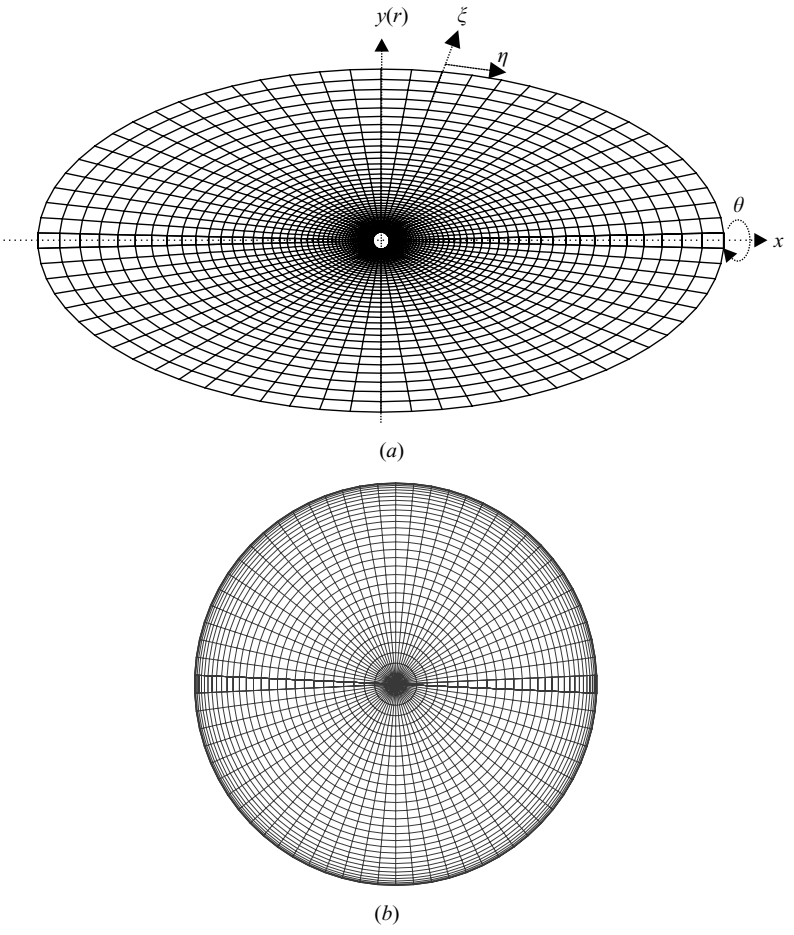

FIGURE 2. Schematic diagram of computational domains: (*a*) outside and (*b*) inside a spherical bubble.

(2002) and different from the definition based on the volume of a sphere by Auton (1987) and Legendre & Magnaudet (1998). The drag and lift coefficients induced by the pressure are called the pressure drag and lift coefficients, while the drag and lift coefficients induced by the viscous stress are called as the viscous drag and lift coefficients.

Numerical grids outside and inside a spherical bubble are shown in figures 2(*a*) and 2(*b*). The (x, r, θ)-coordinate system was transferred to the (η, ξ, θ)-coordinate system with equal spacing. In this study, the size of the computational domain was 20 and 10 diameters in the x- and r-direction, respectively. The size of the computational domain was determined by confirming that difference in the computed results between the present size and the bigger sizes of 50 and 25 diameters in the x- and r-direction is less than 5 % for $Re_p \geqslant 1$. It was also confirmed that the small difference does not affect flow structures and drag and lift forces. The grid points outside a bubble used in this study were $35 \times 61 \times 48$ in η-, ξ- and θ-direction, and the grid points inside a bubble were $35 \times 31 \times 48$. The grid points were determined by confirming that difference in the computed results between the present grid points and the double grid points is less than 4 %.

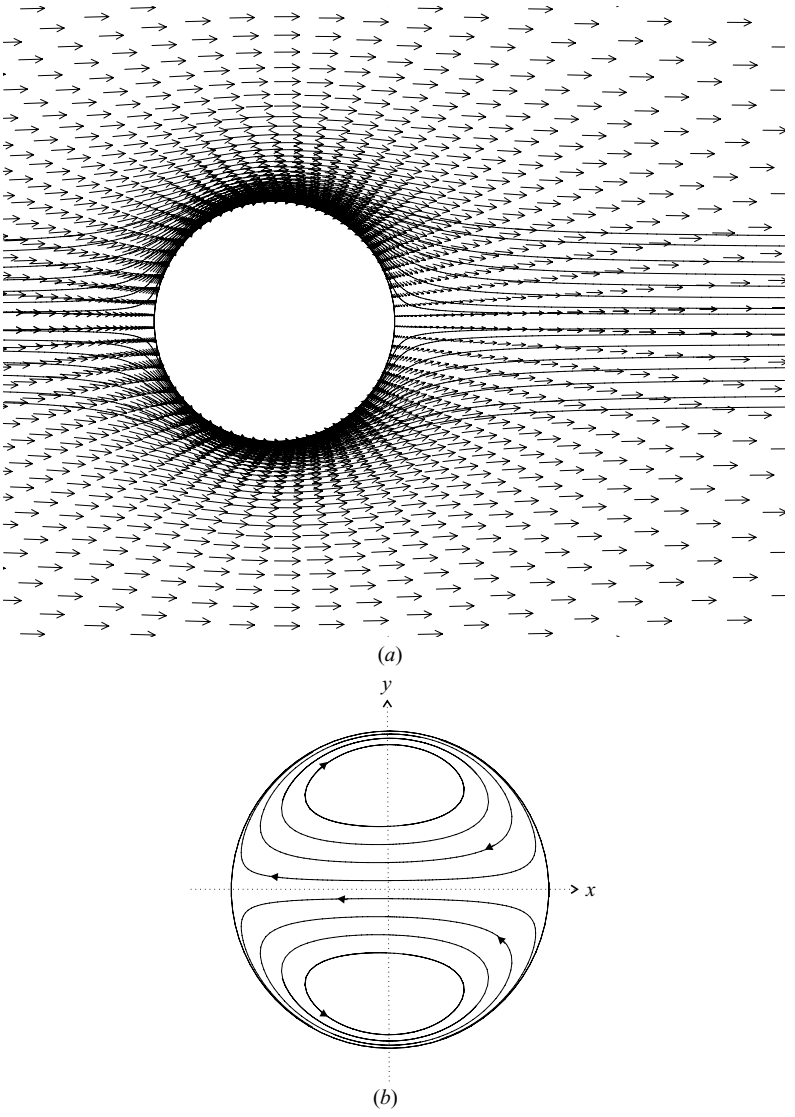

FIGURE 3. Velocity fields and streamlines at $Re_p = 300$ and $\alpha = 0$: (*a*) outside and (*b*) inside a spherical air bubble.

Computations were repeated with a dimensionless time step of $\Delta t = 0.005$ until they almost approached steady state. Similarly, the drag and lift forces on an inviscid bubble were estimated.

The computations for both a spherical gas bubble and a spherical inviscid bubble were performed for particle Reynolds numbers of $Re_p = 1$, 5, 10, 50, 100 and 300 and for fluid shear rates of $\alpha = 0.0$, 0.1, 0.2, 0.3 and 0.4.

3. Results and discussion

3.1. *Flow fields outside and inside a spherical air bubble*

Figures 3(*a*) and 3(*b*) show the velocity fields and streamlines outside and inside a spherical air bubble in a uniform unsheared flow at $Re_p = 300$ and $\alpha = 0$ on the

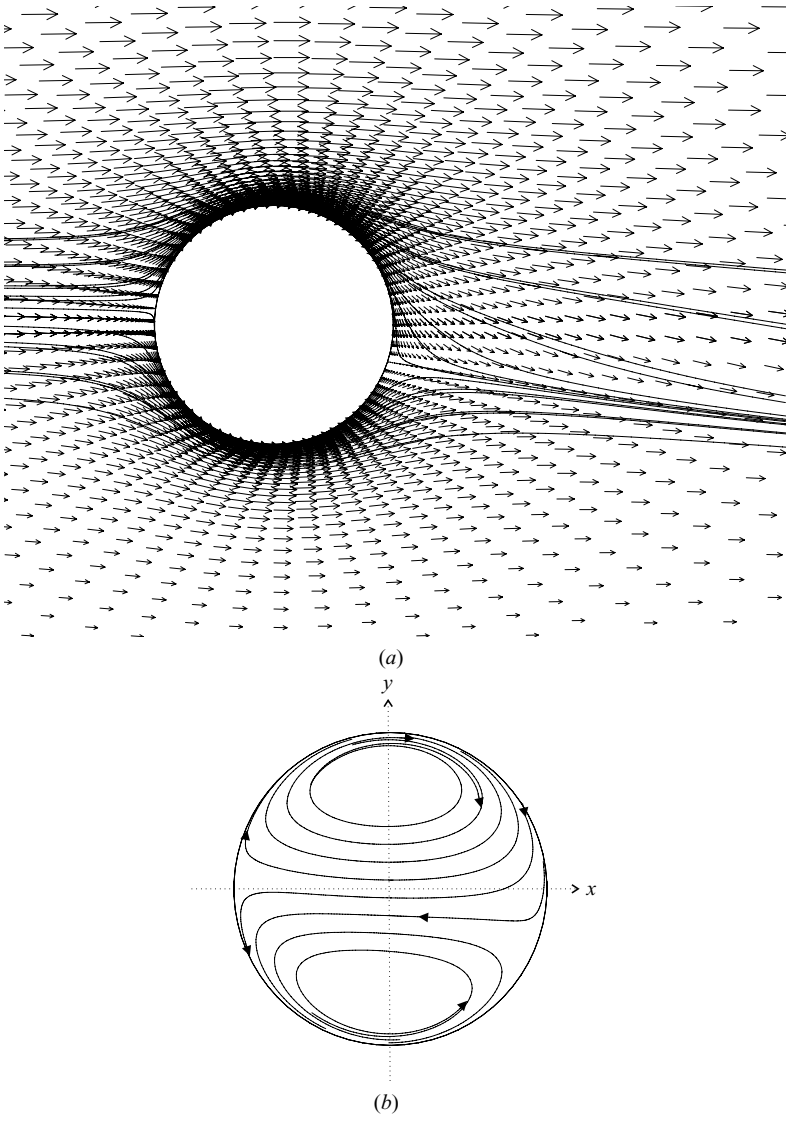

FIGURE 4. Velocity fields and streamlines at $Re_p = 50$ and $\alpha = 0.4$: (*a*) outside and (*b*) inside a spherical air bubble.

centre plane ($z = 0$). It is found that flow separation does not appear behind an air bubble in the ambient flow, and internal air circulations inside an air bubble are generated by the viscous stress acting on the surface of an air bubble. The stagnation points appear at the upstream end and the downstream end of the bubble surface.

Figures 4(*a*) and 4(*b*) show the velocity fields and streamlines outside and inside a spherical air bubble in a linear shear flow for $Re_p = 300$ and $\alpha = 0.4$ on the centre plane ($z = 0$). It is found that flow separation does not appear behind an air bubble in the ambient flow, and the flow in the lower direction is generated behind an air bubble. The internal three-dimensional circulations inside an air bubble are generated by the viscous stress on the surface.

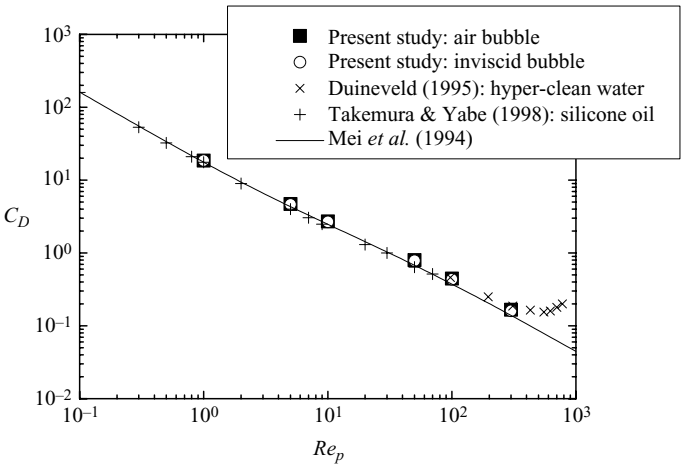

FIGURE 5. Drag coefficient, C_D, on an air bubble and an inviscid bubble in a uniform unsheared flow versus the particle Reynolds number, Re_p.

3.2. *Drag coefficient*

To check the numerical accuracy, the computed drag coefficient C_D was compared with the experimental results and the empirical expression of the drag coefficient C_D. Figure 5 shows the variations of the drag coefficient, C_D, on an inviscid bubble and an air bubble in a uniform unsheared flow against the particle Reynolds number, Re_p. The computed values of C_D on inviscid and air bubbles are compared in figure 5 with the empirical expression for a spherical air bubble by Mei, Klausner & Lawrence (1994) and the experimental results for an air bubble. The symbols $\times$ and $+$ respectively denote the experimental results for an air bubble in 'hyper-clean' water by Duineveld (1995) and an air bubble in silicone oil by Takemura & Yabe (1998). The experimental results by Duineveld for $Re_p > 300$ increase with increasing Re_p owing to deformation of an air bubble. The present DNS predictions for an inviscid bubble and an air bubble are in good agreement with their experimental results and empirical expression in the region of $1 \leqslant Re_p \leqslant 300$ and show that the deformation of an air bubble from the spherical shape is negligibly small in the region of $Re_p \leqslant 300$. This supports the reliability of the present DNS.

Figure 6 shows the ratio of the drag coefficient on an air bubble in a linear shear flow, C_D, to the drag coefficient in a uniform unsheared flow C_{D0} against Re_p. The ratio, C_D/C_{D0}, increases with increase in the dimensionless shear rate α for a fixed value of Re_p, and the dependence of C_D on α is more obvious for higher Re_p. This behaviour is similar to the numerical results for an inviscid bubble by Legendre & Magnaudet (1998). To clarify the difference in the drag between an air bubble and an inviscid bubble, the ratio of the drag coefficient on an air bubble $C_{D,b}$ to that on an inviscid bubble $C_{D,ib}$ is plotted against Re_p in figure 7. Legendre & Magnaudet (1997) showed that in the small particle Reynolds number region of $Re_p \ll 1$, the ratio of C_D on an air bubble to that on an inviscid bubble is 1.01 irrespective of α. They derived this ratio by using the Saffman's (1965) low-Reynolds-number theory that neglected the advection term of the equation of motion. The present results also show that the difference in the drag between an air bubble and an inviscid bubble never exceeds 4 %, and the ratio is almost equal to 1.01 in the parameter space explored in this study.

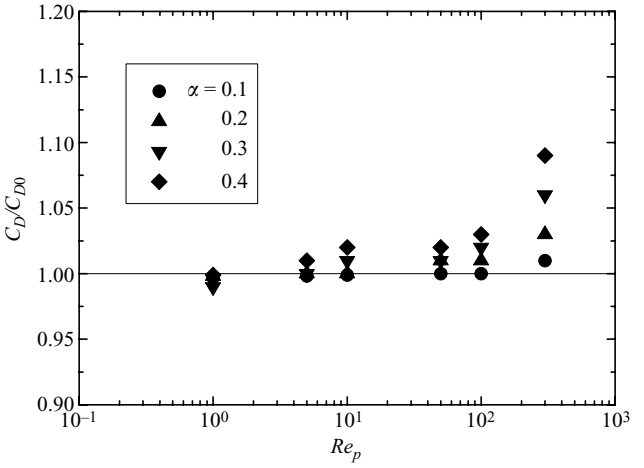

FIGURE 6. The ratio of drag coefficient, C_D, on an air bubble in a linear shear flow to that in a uniform unsheared flow, C_{D0}.

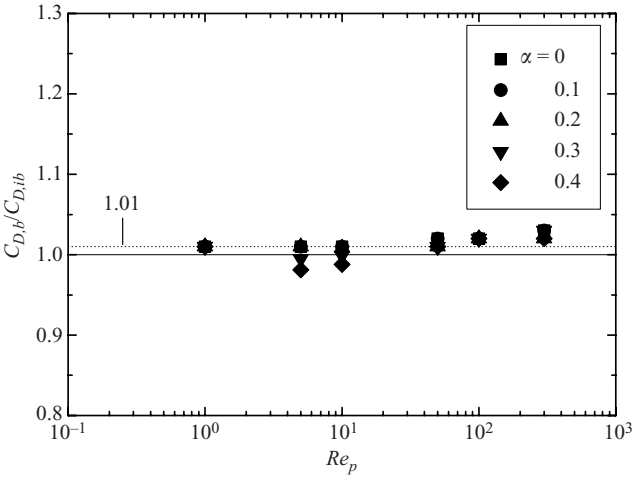

FIGURE 7. The ratio of drag coefficient on an air bubble, $C_{D,b}$, to that on an inviscid bubble, $C_{D,ib}$, in a linear shear flow.

3.3. *Lift coefficient*

Figures 8 and 9 show the variations of lift coefficient, C_L, on a spherical air bubble and a spherical inviscid bubble in linear shear flows for $\alpha = 0.0, 0.1, 0.2, 0.3$ and 0.4 against the particle Reynolds number, Re_p, respectively. The dotted line shown in figures 8 and 9 denotes the lift on a sphere in the non-viscous linear shear flows (Auton 1987) for $\alpha = 0.1, 0.2, 0.3$ and 0.4. The Auton's (1987) lift is given by

$$F_L = \frac{2}{3}\pi\rho\left(\frac{d}{2}\right)^3 \frac{\partial U}{\partial y} U_c. \tag{3.1}$$

The lift coefficient in the Auton's (1987) lift is given in the dimensionless form by

$$C_L = \frac{2}{3}\alpha. \tag{3.2}$$

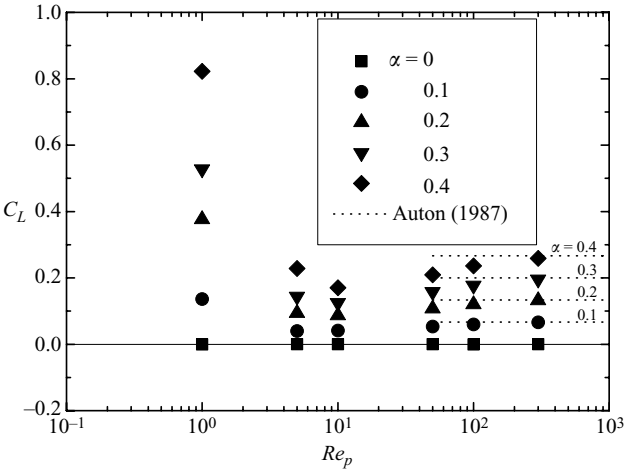

FIGURE 8. Lift coefficient, C_L, on an air bubble versus the particle Reynolds number, Re_p.

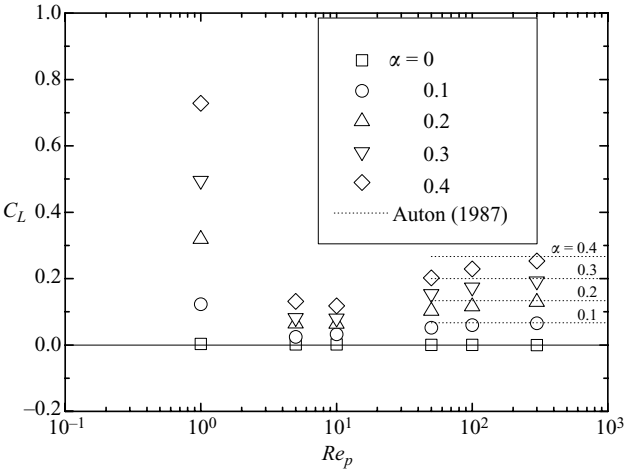

FIGURE 9. Lift coefficient, C_L, on an inviscid bubble versus the particle Reynolds number, Re_p.

The lift force in a uniform unsheared flow ($\alpha = 0$) does not appear ($C_L = 0$) in the case for both an air bubble and an inviscid bubble. The values of C_L on an air bubble and an inviscid bubble in a linear shear flow rapidly decrease with increasing Re_p in the moderate particle Reynolds number range of $Re_p < 10$. At $Re_p = 10$, the values of C_L on an air bubble and an inviscid bubble in a linear shear flow have the minimum peak value. In the high particle Reynolds number range of $Re_p \geqslant 10$, the computed C_L on an air bubble and an inviscid bubble increase to Auton's lift (3.2, Auton 1987). In the cases of a rigid sphere (Kurose & Komori 1999; Bagchi & Balachandar 2002) and a water droplet (Sugioka & Komori 2007) in the linear shear flow, flow separations appear behind a rigid sphere or a water droplet in the high Reynolds number region of $Re_p \geqslant 50$. Therefore, the lift coefficients on a rigid sphere and a water droplet have negative values. However, in the cases of an inviscid bubble (Legendre & Magnaudet 1998; Kurose *et al.* 2001) and an air bubble (see figure 4) in the linear shear flow, flow separation does not appear behind an inviscid bubble and an air bubble even

Re_p	$C_{L,ib}$	$C'_{L,ib}$	$C_{L,b}$	$C'_{L,b}$
1	0.319	1.20	0.376	1.41
5	0.0642	0.241	0.0941	0.353
10	0.0632	0.237	0.0869	0.326
50	0.102	0.383	0.107	0.401
100	0.116	0.435	0.120	0.450
300	0.129	0.484	0.132	0.495

TABLE 2. Lift coefficient on an inviscid bubble, $C_{L,ib}$, and on a spherical air bubble, $C_{L,b}$, for $\alpha = 0.2$; C'_L denotes the the lift coefficient based on the volume of a bubble by Auton (1987) and Legendre & Magnaudet (1998).

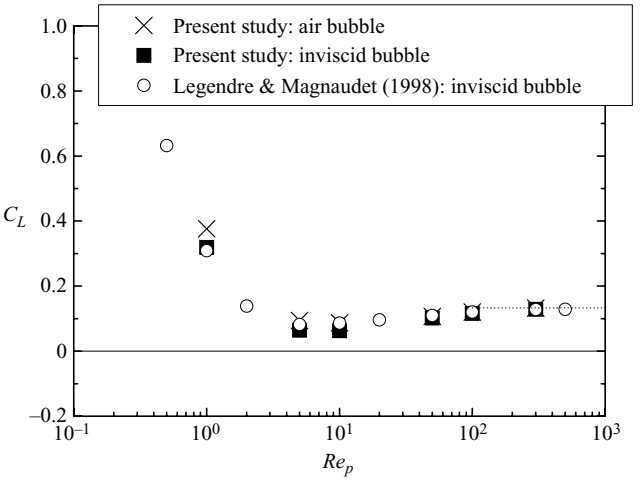

FIGURE 10. Comparison of the lift coefficients, C_L, on a spherical bubble and an inviscid bubble with the result by Legendre & Magnaudet (1998).

in the high-Reynolds-number region. Therefore, the lift coefficients on an inviscid bubble and an air bubble are in agreement with Auton's (1987) lift (3.2). The effects of the shear rate, α, on C_L on an air bubble and an inviscid bubble increase with increasing α. Table 2 shows the value of the lift coefficient on a spherical air bubble $C_{L,b}$ and on an inviscid bubble $C_{L,ib}$ for $\alpha = 0.2$; C'_L denotes the the lift coefficient defined using the volume of a bubble by Auton (1987) and Legendre & Magnaudet (1998). Figure 10 shows the comparison of the lift coefficients, C_L, on a spherical bubble and an inviscid bubble with the lift coefficient by Legendre & Magnaudet (1998) for $\alpha = 0.2$. The lift coefficient on an inviscid bubble is in agreement with the numerical results for an inviscid bubble by Legendre & Magnaudet (1998). However, the effects of the shear rate, α, on C_L on an air bubble are different from those on an inviscid bubble.

To clarify the difference in the lift between an air bubble and an inviscid bubble, the ratio of the lift coefficient on a spherical air bubble, $C_{L,b}$, to that on an inviscid bubble, $C_{L,ib}$, is plotted against Re_p in figure 11. The ratio is bigger than unity for $1 \leqslant Re_p \leqslant 300$. Legendre & Magnaudet (1997) showed that in the small particle Reynolds number region of $Re_p \ll 1$, the ratio of C_L on an air bubble to that on an inviscid bubble is 1.02 irrespective of α. They derived this ratio by using the Saffman's (1965) low-Reynolds-number theory that neglected advection term of the

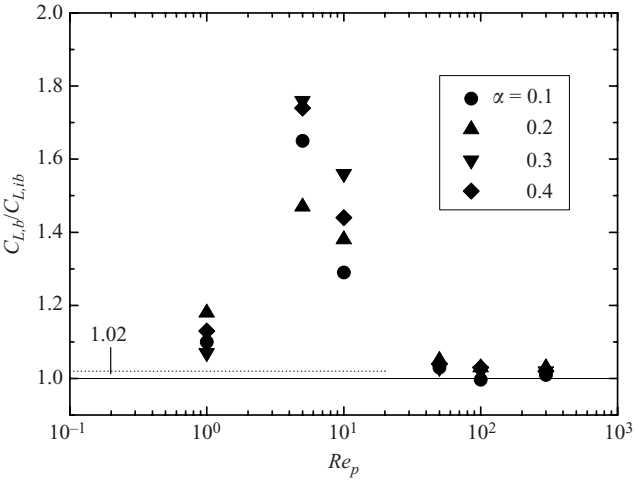

FIGURE 11. The ratio of lift coefficient on an air bubble, $C_{L,b}$, to that on an inviscid bubble, $C_{L,ib}$.

equation of motion. The present results show that the ratio is much bigger than 1.02 for $1 \leqslant Re_p < 50$. This suggests that the low-Reynolds-number theory should not be used for estimating the lift force on a spherical air bubble with $Re_p \geqslant 1$. For $Re_p \geqslant 50$ as the effect of the inertia on the motion of the fluids is much more than that of the viscosity the ratio decreases to unity.

To clarify the detail of the lift coefficient on an air bubble and an inviscid bubble, the viscous and pressure lifts, $C_{L,f}$ and $C_{L,p}$, acting on an air bubble are compared with those acting on an inviscid bubble in figures 12 and 13, respectively. The dotted line shown in figures 13(a) and 13(b) denotes the Auton's lift (3.2) (Auton 1987) for $\alpha = 0.1, 0.2, 0.3$ and 0.4. The values of $C_{L,f}$ on an air bubble and an inviscid bubble in a linear shear flow rapidly decrease with increasing Re_p in the moderate particle Reynolds number range of $Re_p < 10$. At $Re_p = 10$, the values of $C_{L,f}$ on an air bubble and an inviscid bubble in a linear shear flow have the negative minimum peak value. In the high particle Reynolds number range of $Re_p \geqslant 10$, the $C_{L,f}$ on an air bubble and an inviscid bubble increase to zero. The effects of the shear rate, α, on $C_{L,f}$ on an air bubble and an inviscid bubble increase with increasing α. The values of $C_{L,p}$ on an air bubble and an inviscid bubble in a linear shear flow rapidly decrease with increasing Re_p in the moderate particle Reynolds number range of $Re_p < 10$. At $Re_p = 10$, the values of $C_{L,p}$ on an air bubble and an inviscid bubble in a linear shear flow have the positive minimum peak value. In the high particle Reynolds number range of $Re_p \geqslant 10$, the computed $C_{L,p}$ on an air bubble and an inviscid bubble increase to Auton's lift (3.2) (Auton 1987). The effects of the shear rate, α, on $C_{L,p}$ on an air bubble and an inviscid bubble increase with increasing α. To clarify the difference in the viscous and pressure lift between an air bubble and an inviscid bubble, the viscous and pressure lifts, $C_{L,f}$ and $C_{L,p}$, acting on an air bubble are compared with those acting on an inviscid bubble in figures 14 and 15, respectively. In the moderate particle Reynolds number region of $1 \leqslant Re_p < 50$, both the viscous and pressure lift coefficients on an air bubble are much bigger than those on an inviscid bubble. In the high particle Reynolds number region of $50 \leqslant Re_p \leqslant 300$, both the viscous and pressure lift coefficients on an air bubble are slightly bigger than those on an inviscid bubble.

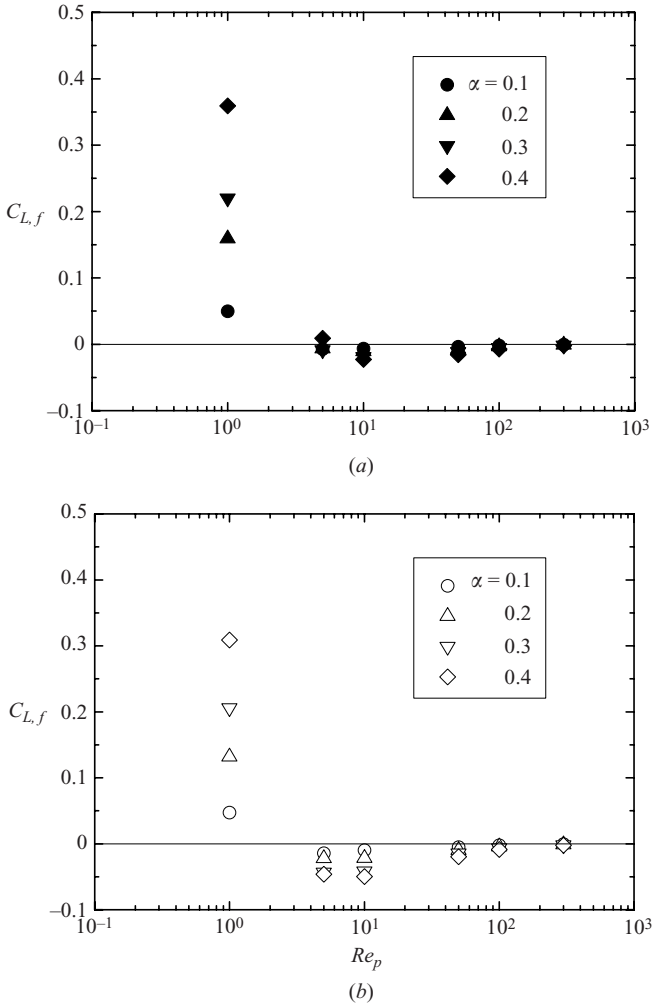

FIGURE 12. Viscous lift coefficient, $C_{L,f}$, versus the particle Reynolds number, Re_p: (*a*) for an air bubble; (*b*) for an inviscid bubble.

To clarify the detail of the viscous and pressure lift coefficients on an air bubble and an inviscid bubble, the distributions of the y-component of the viscous stress and the pressure on the bubble surface at $Re_p = 5$ and $\alpha = 0.4$ are shown for both air and inviscid bubbles in figure 16(*a*) and figure 16(*b*), respectively. The values of $\phi = 0$ and $\phi = \pi$ correspond to the upstream and downstream ends of the bubble surface, respectively. The values of $\theta = 0$, $\theta = 0.5\pi$ and $\theta = \pi$ correspond to the upper, centre and lower sides of the bubble surface, respectively. The surface-averaged values of the viscous stress on the upper ($\theta = 0$) and lower ($\theta = \pi$) sides become small in both air and inviscid bubble cases, since the negative parts are almost balanced by the positive parts. Therefore, the viscous lift coefficients on an air bubble and an inviscid bubble at $Re_p = 5$ and $\alpha = 0.4$ are almost zero as shown in figure 14. The large part of the positive pressure on the upper side ($\theta = 0$) in the middle and downstream regions ($\phi \geqslant 0.4\pi$) leads to the positive pressure lift coefficients on an air bubble and an inviscid bubble as shown in figure 15. The distributions of the y-component of the viscous stress and the pressure on the air bubble surface are quite similar to those

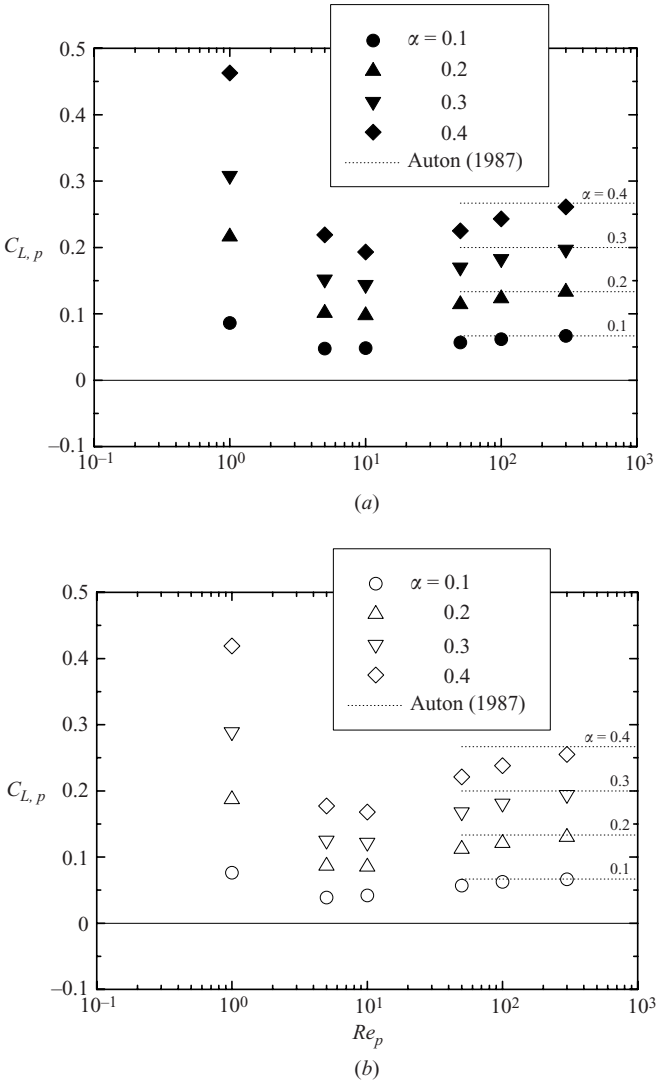

FIGURE 13. Pressure lift coefficient, $C_{L,p}$, versus the particle Reynolds number, Re_p: (*a*) for an air bubble; (*b*) for an inviscid bubble.

on the inviscid bubble surface. To clarify the difference in the local viscous stress and the pressure between an air bubble and an inviscid bubble, figures 17(*a*) and 17(*b*) show the distributions of the difference in the y-component of the viscous stress and the pressure on the surface between an air bubble and an inviscid bubble at $Re_p = 5$ and $\alpha = 0.4$, respectively. The surface-averaged difference in the viscous stress on the upper side and the centre ($\theta = 0,\ 0.5\pi$) is almost zero, whereas the surface-averaged difference in the viscous stress on the lower side ($\theta = \pi$) is positive. Therefore, the viscous lift coefficient on an air bubble is bigger than that on an inviscid bubble. The surface-averaged difference in pressure on the centre ($\theta = 0.5\pi$) is almost zero, whereas the surface-averaged difference in pressure on both the upper and lower sides ($\theta = 0,\ \pi$) is positive. Therefore, the pressure lift coefficient on an air bubble is bigger than that on an inviscid bubble.

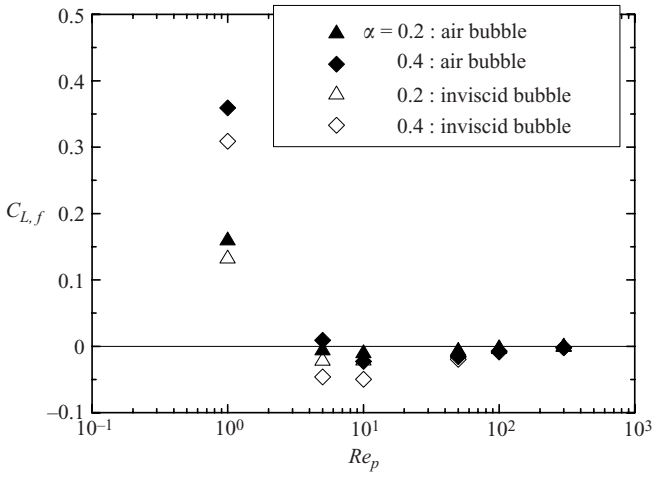

FIGURE 14. Viscous lift coefficient on an air bubble and an inviscid bubble, $C_{L,f}$, for $\alpha = 0.2$ and 0.4.

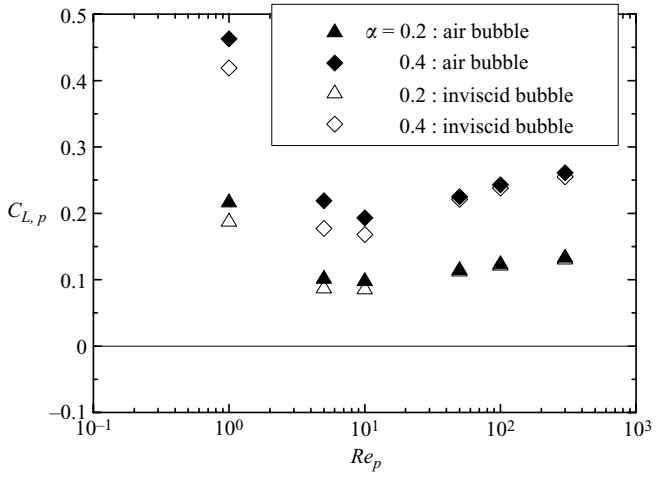

FIGURE 15. Pressure lift coefficient on an air bubble and an inviscid bubble, $C_{L,p}$, for $\alpha = 0.2$ and 0.4.

Figure 18 shows the tangential velocity v_ϕ on the surface of an air bubble and an inviscid bubble at $Re_p = 5$ and $\alpha = 0.4$. In both the upper ($\theta = 0$) and lower ($\theta = \pi$) sides, the tangential velocity on the surface of an air bubble is slightly less than that of an inviscid bubble. The viscosity of the air-flow inside an air bubble causes the suppression of the surface velocity. The suppression of the surface velocity increases the viscous and pressure lifts on an air bubble.

3.4. *Fluid force on a viscous bubble*

To clarify the effect of the ratio of fluid viscosities inside and outside a bubble on the fluid force, the viscosity ratio is set to the values of 10, 0.2 and 0.1 times that of an air bubble in water. These respectively correspond to gas bubbles with 0.1, 5 and 10 times the air viscosity in water flow or air bubbles in the liquid flow with 10, 0.2 and 0.1 times the water viscosity. A bubble with quintuple air viscosity is, hereafter, called 'a highly viscous bubble'. Figure 19 shows the ratio of the drag coefficient on a

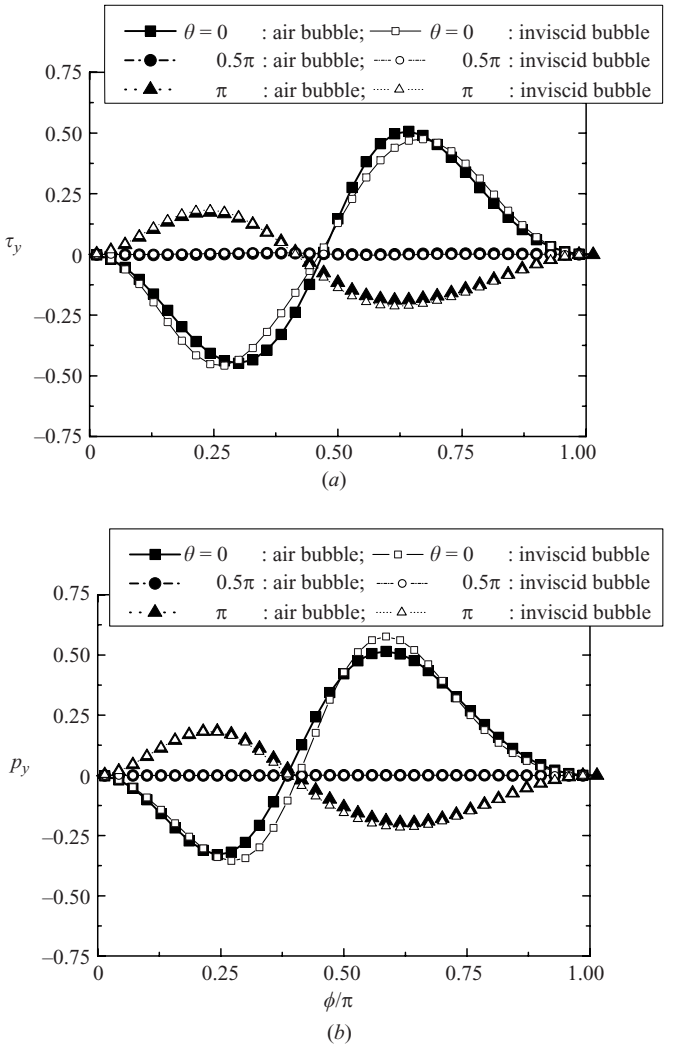

FIGURE 16. Distribution of the y-component of the viscous stress and the pressure on the surface at $Re_p = 5$ and $\alpha = 0.4$: (a) viscous stress, $\boldsymbol{\tau}_y$; (b) pressure, p_y.

highly viscous bubble $C_{D,vb}$ to that on an inviscid bubble, $C_{D,ib}$, against the particle Reynolds number, Re_p. The dotted line denotes the value of $C_{D,vb}/C_{D,ib}$ given by Legendre & Magnaudet (1997). The ratio is bigger than unity. This suggests that the drag coefficient on a highly viscous bubble becomes bigger than that on an inviscid bubble. The effect of the shear rate of the ambient flow on the drag coefficient on a highly viscous bubble is more obvious than that on an air bubble shown in figure 7. The ratio of drag coefficients is almost equal to 1.046 in the parameter space explored in this study. These suggest that the internal gas viscosity increases the drag coefficient.

Figure 20 shows the ratio of the lift coefficient on a highly viscous bubble, $C_{L,vb}$, to that on an inviscid bubble, $C_{L,ib}$, against the particle Reynolds number, Re_p. To compare the lift coefficient on a highly viscous bubble with that on an air bubble, the lift coefficient on an air bubble is also referred from figure 11. The ratio of the lift

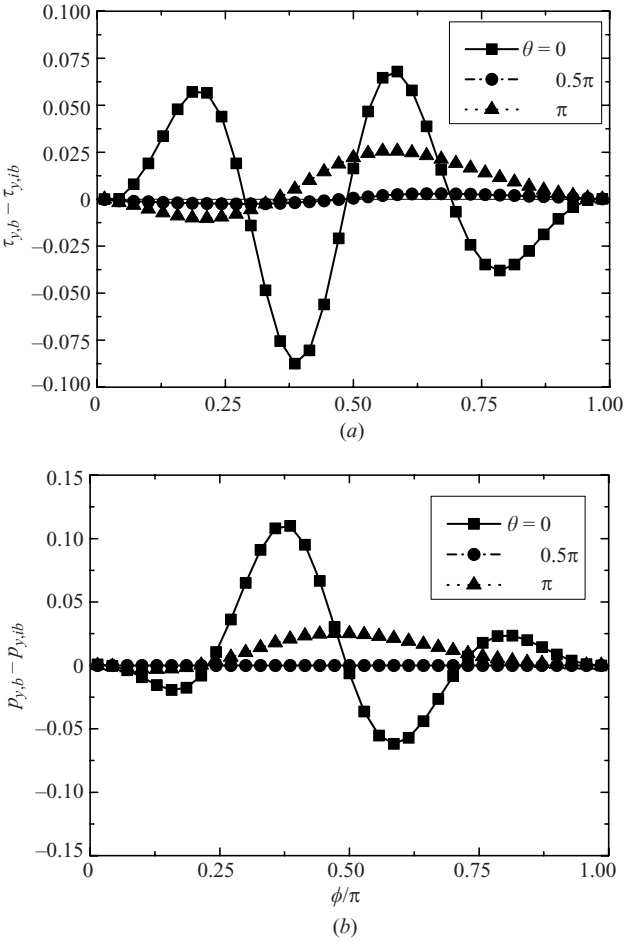

FIGURE 17. Distribution of the difference in the y-component of the viscous stress and the pressure between an air bubble and an inviscid bubble at $Re_p = 5$ and $\alpha = 0.4$: (a) viscous stress, $\boldsymbol{\tau}_{y,b} - \boldsymbol{\tau}_{y,ib}$; ($b$) pressure, $p_{y,b} - p_{y,ib}$.

coefficients for a highly viscous bubble, $C_{L,vb}/C_{L,ib}$, given by Legendre & Magnaudet (1997) is 1.095. The present results show that the ratio for a highly viscous bubble is much bigger than 1.095 for $5 \leqslant Re_p < 50$. This also suggests that the low-Reynolds-number theory should not be used for estimating the lift force on a spherical air bubble with $Re_p \geqslant 5$. Moreover, the present results show that the lift coefficient on a highly viscous bubble is smaller than that on an air bubble for $Re_p \geqslant 5$. To clarify the effect of the internal gas viscosity on the lift coefficient, figure 21 shows the relation between the viscosity ratio of the outside and inside fluids, μ_o/μ_i, and the ratio of the lift coefficient on a bubble, C_L, to that on an inviscid bubble, $C_{D,ib}$, for $\alpha = 0.4$. The solid and open symbols respectively denote the lift coefficient on a gas bubble in this study and a water droplet in the linear shear airflow referred from Sugioka & Komori (2007). The case of the extremely low gas viscosity of $\mu_o/\mu_i = \infty$ corresponds to the case of an inviscid bubble and the extremely high-gas-viscosity case of $\mu_o/\mu_i = 0$ corresponds to the case of a rigid sphere. The lift coefficient on a spherical bubble becomes smaller with increasing the viscosity ratio at $Re_p = 1$ and

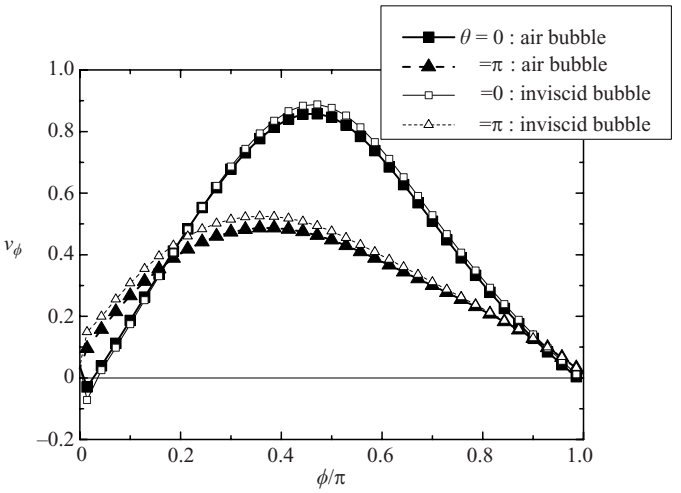

FIGURE 18. Tangential velocity on the surface of an air bubble and an inviscid bubble at $Re_p = 5$ and $\alpha = 0.4$.

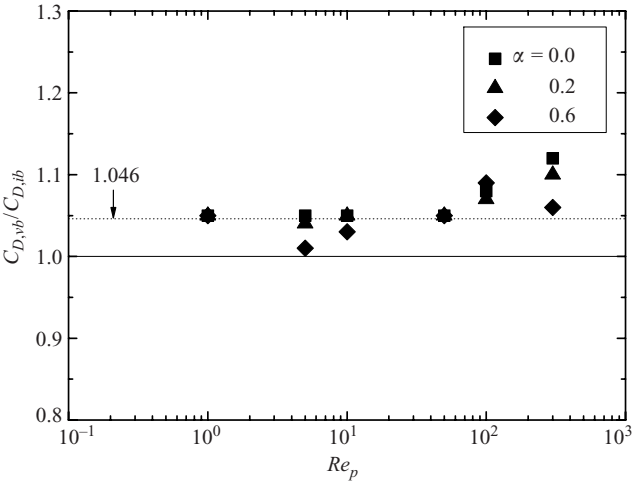

FIGURE 19. The ratio of the drag coefficient on a highly viscous bubble, $C_{D,vb}$, to that on an inviscid bubble, $C_{D,ib}$.

becomes larger with increasing the viscosity ratio in the range of $Re_p \geqslant 5$. At $Re_p = 1$, the lift coefficient on a gas bubble is smaller than that on a water droplet in the linear shear airflow and bigger than that on a water droplet in the linear shear airflow in the range of $Re_p \geqslant 5$. These suggest that the lift coefficient on a gas bubble approaches the lift coefficient on a water droplet in the linear shear airflow with decreasing the viscosity ratio, i.e. increasing the internal gas viscosity.

4. Conclusions

A three-dimensional DNS was first performed for a linear shear flow outside and inside a spherical gas bubble with high particle Reynolds number, and the effects of fluid shear on drag and lift forces were investigated by comparing with the DNS

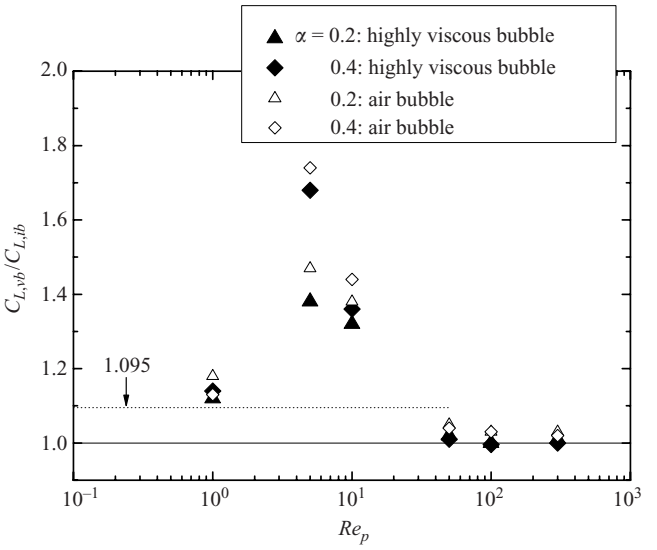

FIGURE 20. The ratio of the lift coefficient on a highly viscous bubble, $C_{L,vb}$, to that on an inviscid bubble, $C_{L,ib}$.

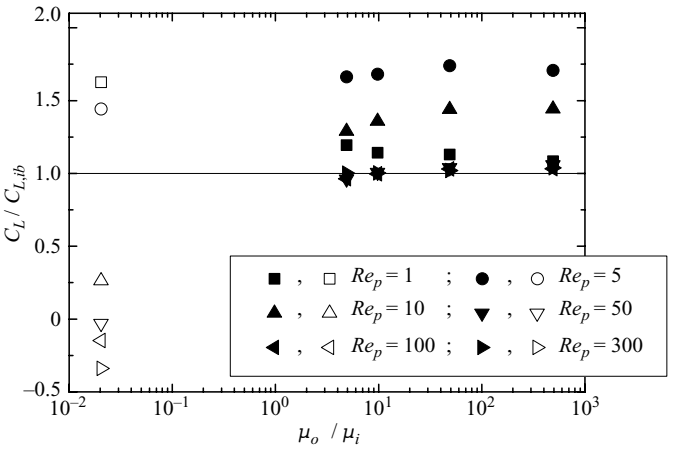

FIGURE 21. The relation between the viscosity ratio and the ratio of the lift coefficient on a bubble, C_L, to that on an inviscid bubble, $C_{L,ib}$, for $\alpha = 0.4$. The solid and open symbols respectively denote the lift coefficient on a gas bubble in this study and a water droplet in the linear shear airflow referred from Sugioka & Komori (2007).

predictions of a spherical inviscid bubble. The main results from this study can be summarized as follows: The drag coefficient on an air bubble increases with increasing shear rate, and the dependence of the drag coefficient on the shear rate is more obvious for higher particle Reynolds numbers. The difference in the drag between an air bubble and an inviscid bubble in a linear shear flow never exceeds 4 % in the parameter space explored in this study.

The lift coefficient on an air bubble decreases with increasing the particle Reynolds number in the moderate particle Reynolds number range of $Re_p < 10$. At $Re_p = 10$, the values of the lift coefficient on an air bubble in a linear shear flow have the minimum peak value. In the high particle Reynolds number range of $Re_p \geqslant 10$,

the lift coefficients on both air and inviscid bubbles increase to two thirds of the dimensionless fluid shear rate of the mean flow. The behaviour of the lift force on an air bubble is similar to that on an inviscid bubble, but the effects of fluid shear rate on the lift coefficient acting on an air bubble in the linear shear flow become bigger than those acting on an inviscid bubble. The lift force on an air bubble is 50 %–80 % bigger than that on an inviscid bubble at $Re_p = 5$ and is 30 %–60 % bigger at $Re_p = 10$. In the ranges of $Re_p \simeq 1$ and $50 \leqslant Re_p \leqslant 300$, the difference becomes less obvious. The difference is attributed to the increase of the viscous and pressure lifts on an air bubble that are caused by the air viscosity inside the spherical bubble.

The lift coefficient on a gas bubble approaches the lift coefficient on a water droplet in the linear shear airflow with increasing the internal gas viscosity.

This work was supported by the Japan Ministry of Education, Science and Culture through grants-in-aid 19206023 and 20760118. The computations were conducted by the supercomputer of the Center for the Global Environment Research, National Institute for Environmental Studies, Environment Ministry of Japan.

REFERENCES

Auton, T. R. 1987 The lift force on a spherical body in a rotational flow. *J. Fluid Mech.* **183**, 199–218.

Bagchi, P. & Balanchandar, S. 2002 Effect of rotation on the motion of a solid sphere in linear shear flow at moderate *Re*. *Phys. Fluids.* **14**, 2719–2737.

Dandy, D. & Dwyer, H. A. 1990 A sphere in linear shear flow at finite Reynolds number: effect of shear on particle lift, drag, and heat transfer. *J. Fluid Mech.* **216**, 381–410.

Duineveld, P. C. 1995 The rise velocity and shape of bubbles in pure water at high Reynolds number. *J. Fluid Mech.* **292**, 325–332.

Fdhila, R. B. & Duineveld, P. C. 1996 The effect of surfactant on the rise of a spherical bubble at high Reynolds and Peclet numbers. *Phys. Fluids* **8**, 310–321.

Hanazaki, H. 1988 A numerical study of three-dimensional stratified flow past a sphere. *J. Fluid Mech.* **192**, 393–419.

Komori, S. & Kurose, R. 1996 The effects of shear and spin on particle lift and drag in a shear flow at high Reynolds numbers, In *Advances in Turbulence VI* (ed. S. Gavrilakis, L. Machiels & P. A. Monkewitz), pp. 551–554. Kluwer.

Kurose, R. & Komori, S. 1999 Drag and lift force on a rotation sphere in linear shear flow. *J. Fluid Mech.* **384**, 183–206.

Kurose, R., Misumi, R. & Komori, S. 2001 Drag and lift forces acting on a spherical bubble in a linear shear flow. *Intl J. Multiphase Flow* **27**, 1247–1258.

Leal, L. G. 1980 Particle motions in a viscous fluid. *Annu. Rev. Fluid Mech.* **12**, 435–476.

Legendre, D. & Magnaudet, J. 1997 A note on the lift force on a spherical bubble or drop in a low-Reynolds-number shear flow. *Phys. Fluids* A **9** (11), 3572–3574.

Legendre, D. & Magnaudet, J. 1998 The lift force on a spherical bubble in a viscous linear shear flow. *J. Fluid Mech.* **368**, 81–126.

Maxworthy, T., Gnann, C., Kürten, M. & Durst, F. 1996 Experiments on the rise of air bubbles in clean viscous liquids. *J. Fluid Mech.* **321**, 421–441.

McLaughlin, J. B. 1993 The lift on a small sphere in wall-bounded linear shear flows. *J. Fluid Mech.* **246**, 249–265.

Mei, R., Klausner, J. F. & Lawrence, C. J. 1994 A note on the history force on a spherical bubble at finite Reynolds number. *Phys. Fluids* **6**, 418–420.

Palaparthi, R., Demetrios, T. P. & Maldarelli, C. 2006 Theory and experiments on the stagnant cap regime in the motion of spherical surfactant-laden bubbles. *J. Fluid Mech.* **559**, 1–44.

Saffman, P. G. 1965 The lift on a small sphere in a slow shear flow. *J. Fluid Mech.* **22**, 385–400.

Sankaranarayanan, K., Shan, X., Kerekidis, I. G. & Sundaresan, S. 2002 Analysis of drag and virtual mass forces in bubbly suspensions using an implicit formulation of the lattice Boltzmann method. *J. Fluid Mech.* **452**, 61–96.

Sankaranarayanan, K. & Sundaresan, S. 2002 Lift force in bubbly suspensions. *Chem. Engng Sci.* **57**, 3521–3542.

Sugioka, K. & Komori, S. 2007 Drag and lift forces acting on a spherical water droplet in homogeneous linear shear air flow. *J. Fluid Mech.* **570**, 155–175.

Takemura, F. & Yabe, A. 1998 Gas dissolution process of spherical rising gas bubbles. *Chem. Engng Sci.* **53** (15), 26891–2699.

Takemura, F. & Yabe, A. 1999 Rising speed and dissolution rate of a carbon dioxide bubble in slightly contaminated water. *J. Fluid Mech.* **378**, 319–334.

Wohl, P. R. & Rubinow, S. I. 1974 The transverse force on a drop in an unbounded parabolic flow. *J. Fluid Mech.* **62**, 185–207.